Korean J. Chem. Eng., 37(5), 883-890 (2020)
DOI: 10.1007/s11814-019-0461-1

pISSN: 0256-1115
eISSN: 1975-7220

Multi-objective optimization model of high-temperature ceramic filter

Longfei Liu*,, Zhongli Ji*,**,†, and Xin Luan*,****

*Department of Mechanical and Transportation Engineering, China University of Petroleum, Beijing 102249, China
**Beijing Key Laboratory of Process Fluid Filtration and Separation, China University of Petroleum, Beijing 102249, China
(*Received 26 September 2019 • accepted 9 December 2019*)

Abstract−Ceramic filters have been widely used in industrial engineering, such as the Shell coal gasification process (SCGP) and Integrated gasification combined cycle (IGCC), where the performance of the ceramic filter is achieved by the pulse jet. Residual pressure drop and gas consumption are directly related to reverse-flow pulse (RFP) pressure. However, in the process of operation, the RFP pressure is too large and gas consumption is too high. In this study, the effects of RFP pressures on filter's cleaning efficiency, residual pressure drop, and gas consumption were investigated on a ceramic filter. Within a certain range, the cleaning efficiency gradually increased with increased RFP pressure. When the RFP pressure reached a certain value, the cleaning efficiency did not increase with increased pressure, showing a quadratic relationship between cleaning efficiency and RFP pressure. The residual pressure drop and RFP pressure were also in a quadratic relationship. Besides, the gas consumption increased linearly as increased RFP pressure according to the theoretical model. Based on the research results, a multi-objective optimization model of a ceramic filter was established with the cleaning efficiency as a constraint condition, gas consumption and residual pressure drop as the optimization objectives. A fuzzy decision-making method was used to solve the optimization model and calculate the residual pressure drop and gas consumption, from which the optimal RFP pressure was obtained.

Keywords: Ceramic Filter Tube, Reverse-flow Pulse Pressure, Multi-objective Optimization, Fuzzy Decision-making Method

INTRODUCTION

Ceramic filters have been widely used in integrated gasification combined cycle, pressurized fluidized bed combustion, biomass gasification and waste incineration [1-3]. It is the most effective way to remove dust in high temperature environments [4]. The performance of ceramic filter tubes is directly related to filtration system stability; cleaning efficiency is directly related to the magnitude of the reverse-flow pulse (RFP) pressure. When the RFP pressure is too small, a portion of dust will be removed and dust bridging will occur, which can cause serious filter tube fracturing. If the RFP pressure is too high, a portion of dust, which is separated from the filter tube, will rise again to the filter tube. As the pulse jet process is about to end and the filtration process is not yet established, there is a negative pressure zone inside the filter tube which can cause some fine dust to be redeposit to the filter tube surface, thus reducing cleaning efficiency [5-7]. Lupion et al. studied the effects of RFP pressure and pulse jet interval on cleaning efficiency in the range of 230-550 °C and found that cleaning efficiency and the pulse jet interval did not increase with increased RFP pressure [8,9]. Bakke took cleaning energy into account, using filter rate versus grain loading curve at a given pressure drop and filter rate versus pressure drop at a given grain loading curve to optimize filtration parameters [10]. Ju et al. took the economic factor into consideration, established the multiple-objective model by using predictive control technique [11]; the simulation showed the model was suitable for the pulse jet filtration process. Ji et al. took the transient flow method and established the gas consumption prediction model. The model could predict gas consumption under different RFP pressures, found gas consumption increased with the RFP pressure [12]. It was found that RFP pressure was related to filtration velocity; the higher the filtration velocity, the denser filter cake on the surface, and therefore the higher RFP pressure was needed. An excessive RFP pressure could cause small particles to redeposit on the candle surface, resulting in a thinner and denser layer, leading to higher residual pressure drop [13]. Scholars have done extensive research on pulse-jet systems, but no model has been established with optimization of gas consumption and residual pressure drop, so the optimal RFP pressure is not clear.

We performed experiments and calculated the efficiency and residual pressure drop of a ceramic filter under different RFP pressures. A multi-objective optimization model of ceramic filter was established to obtain the optimal RFP pressure by taking cleaning efficiency as the constraint condition, gas consumption and residual pressure drop as the objective function.

EXPERIMENTAL

A schematic diagram of the experimental set-up is shown in Fig. 1 according to VDI 3926. Fifteen type DS 10-20 ceramic filter elements with an outer diameter of 60 mm, inner diameter of 40 mm, and length of 1,500 mm (Pall Co.) were installed in the filter. The elements were divided into five groups and each group shared one ejector.

Dusty gas entered the filter and reached filter element surfaces through a riser and gas distributor. The dust was trapped on the sur-

†To whom correspondence should be addressed.
E-mail: jizhongli63@vip.sina.com

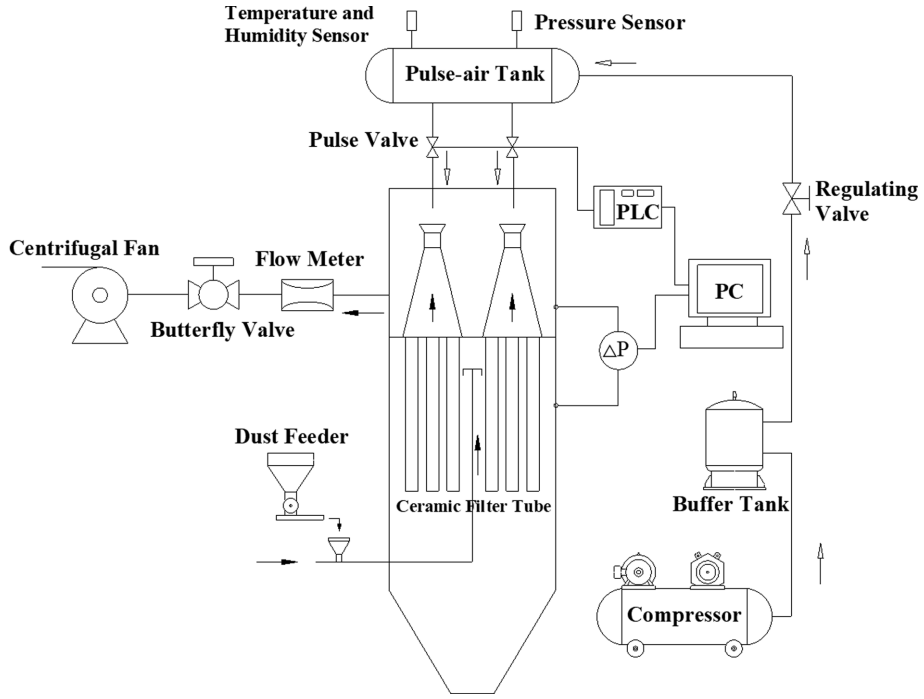

Fig. 1. Schematic diagram of the experimental set-up.

face of the filter element and formed a dust layer; the ceramic filter element was cleaned by the pulse jet as filtration continued. The pulse valve was controlled by a programmable logic controller (PLC) and quickly opened for pulse jet cleaning. Cleaning gas was ejected and entered the filter element, removing the dust layer and regenerating the performance of the ceramic filter element. The filter facilitated gas flow via a centrifugal fan, gas flow was controlled by an electric butterfly valve via the proportion-integral-derivative (PID) method.

As the pulse jet process was completed in a very short time (milliseconds), the process of ejecting high-speed and high-pressure gas from the pulse air tank was considered to be an adiabatic process. The equation for calculating gas consumption is as follows:

$$G=\frac{p_a V}{\mathrm{R}T_1}\left[1-\left(\frac{p_b}{p_a}\right)^{\frac{1}{\gamma}}\right] \tag{1}$$

where G is the gas consumption for each pulse jet, g; p_a and p_b are the absolute pressure of the pulse air tank before and after pulse jet, respectively, Pa; T_1 is the gas temperature before pulse jet, K; V is the pulse air tank volume, m^3; γ is the adiabatic exponent, 1.4; R is the gas characteristic constant, 287 $m^2 \cdot s^{-2} \cdot K^{-1}$.

The cleaning efficiency is defined as the difference between the maximum pressure drop and the residual pressure drop, just after the pulse is given, in relation to the difference between maximum pressure drop and initial pressure drop [14]. The equation is as follows:

$$\eta=\frac{\Delta p_a-\Delta p_a}{\Delta p_d-\Delta p_0} \tag{2}$$

where η is the filter cleaning efficiency; Δp_d and Δp_a are the pressure drops of the ceramic filter tubes before and after pulse jet; Δp_0 is the initial pressure drop of the ceramic filter tubes.

Table 1. Experimental parameters

Parameter	Value
Inlet concentration	5 g/m^3
Type of dust	Fly ash
Reverse-flow pulse pressure	0.15, 0.30, 0.45, 0.60, and 0.75 MPa
Filtration velocity	1 m/min
Pulse width	350 ms
Pulse jet interval	30 min

Research showed that changing the pulse width had no effect on cleaning efficiency but it increased gas consumption [12]. Therefore, the 350 ms pulse width was selected during the experiment as used in industrial applications.

The experimental parameters and dust in the experiment are shown in Table 1. The volume median diameter of dust was 4.123 μm.

RESULTS AND DISCUSSION

Under pure air-flow condition, the initial pressure drop of the clean filter tube was obtained by changing the filtration velocity, as shown in Fig. 2.

The relationship between the initial filter tube pressure drop and filtration velocity was as follows after data fitting.

$$\Delta p_0=0.794v-0.381 \tag{3}$$

where Δp_0 is the initial filter tube pressure drop and v is the filtra-

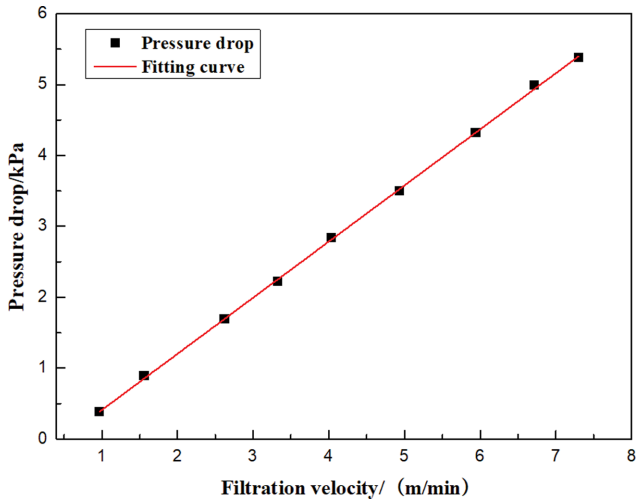

Fig. 2. Initial pressure drop of the ceramic filter tube.

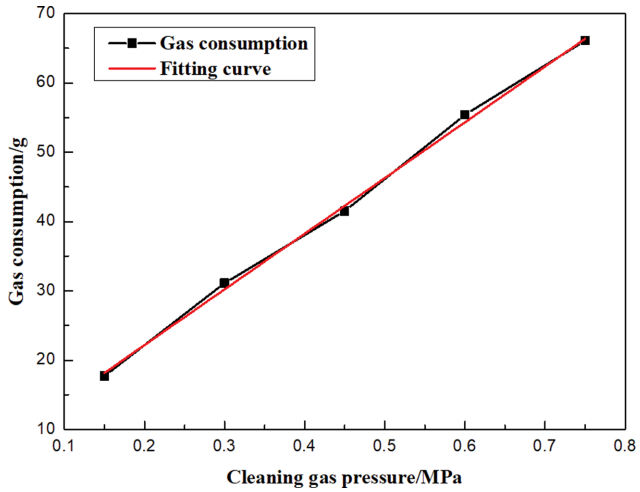

Fig. 3. Gas consumption under different RFP pressures.

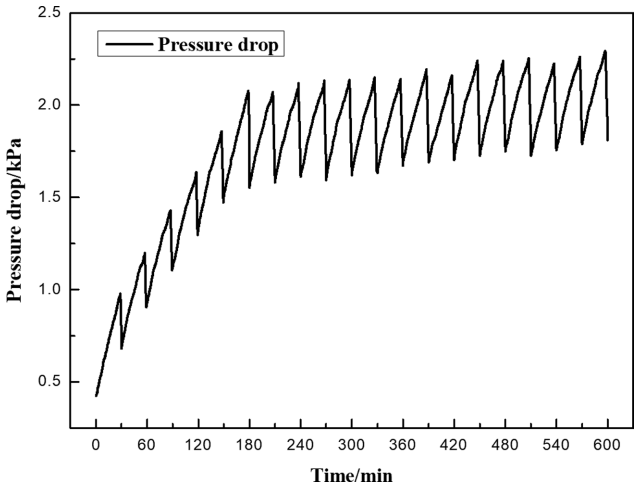

Fig. 4. Influence of 0.15 MPa RFP pressure on pressure drop evolution.

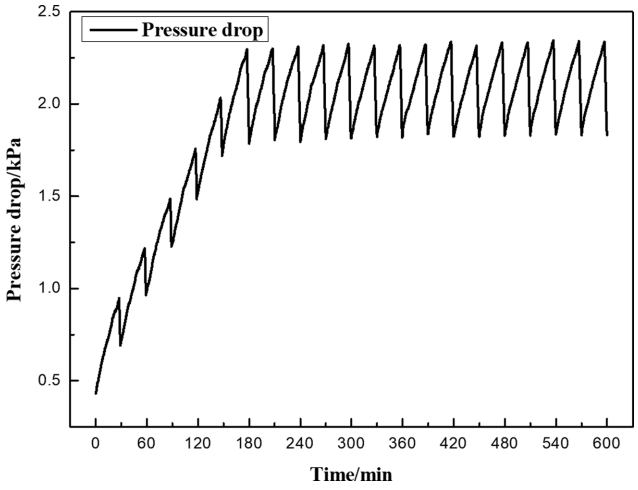

Fig. 5. Influence of 0.30 MPa RFP pressure on pressure drop evolution.

tion velocity. It was known that the initial filter tube pressure drop was 0.413 kPa from Eq. (3) when the filtration velocity was 1 m/min.

By measuring the temperature and pressure of the pulse air tank before and after the pulse jet under different RFP pressures, gas consumption was calculated using Eq. (2). Gas consumption was obtained from the average of five experiments, as shown in Fig. 3.

When the experimental nozzle, pipe size, pressure tank volume, and pulse width were constant, gas consumption was linearly related to the RFP pressure. The calculation results were consistent with the results of gas consumption model established by Ji [12]. The relationship between the gas consumption and RFP pressure was:

$$G=80.72p_1+6.11 \quad (4)$$

where G is the gas consumption and p_1 is the RFP pressure.

1. Effects of RFP Pressure

The filter pressure drop was composed of a base pressure drop in the filter tube, residual dust layer drop, and temporary dust layer drop; the residual pressure drop is the sum of base pressure drop and residual dust layer pressure drop [15]. One cycle in the experiment referred to the interval between two groups of filter tubes for cleaning. As only one group of filter tubes could be cleaned at a time, the sum of the pressure drops after cleaning one group and the other four groups of normal filtration was called the residual pressure drop in this paper. The cleaning efficiency was calculated from the sixth cycle.

The filter tube pressure drop at an RFP pressure of 0.15 MPa for a total of 20 cycles showed that the residual filter tube pressure drop was unstable, as can be seen from Fig. 4. After 20 cycles, the residual pressure drop still exhibited a rising trend, indicating that it could not meet the cleaning requirements when the RFP pressure was 0.15 MPa.

Fig. 5 is the filter tube pressure drop at the RFP pressure of 0.30 MPa for a total of 20 cycles; it shows that the residual filter tube pressure drop was stable and did not increase as the filtration time progressed. It could meet the cleaning requirement at RFP pressure of 0.3 MPa, but the residual pressure drop was high.

Table 2. Influence of 0.3 MPa RFP pressure on cleaning efficiency

Cycling time	Residual pressure drop (kPa)	Cleaning efficiency (%)	Cycling time	Residual pressure drop (kPa)	Cleaning efficiency (%)
6	1.786	23.9	14	1.829	23.3
7	1.806	23.1	15	1.822	22.9
8	1.795	24.1	16	1.829	23.2
9	1.811	23.5	17	1.829	23.4
10	1.814	23.6	18	1.836	23.2
11	1.822	22.8	19	1.831	23.3
12	1.824	22.4	20	1.833	23.1
13	1.840	22.9			

The cleaning efficiency of each cycle at the RFP pressure of 0.3 MPa was calculated using Eq. (2) and shown in Table 2. The residual pressure drop after each cycle at 0.30 MPa RFP pressure was obtained in Fig. 5. The average cleaning efficiency calculated at an RFP pressure of 0.30 MPa was 23.3%.

Fig. 6 is the filter tube pressure drop at the RFP pressure of 0.45 MPa for a total of 20 cycling times; it shows that the residual filter tube pressure drop was stable and did not increase as the filtration time progressed. It could meet the cleaning requirement at RFP pressure of 0.45 MPa, and the residual pressure drop was lower than the residual pressure drop when the RFP pressure was 0.30 MPa.

According to Eq. (2), the cleaning efficiency of each cycle at an RFP pressure of 0.45 MPa was calculated (Table 3). The residual pressure drop after each cycle at 0.45 MPa RFP pressure was obtained. The average cleaning efficiency calculated at an RFP pressure of 0.45 MPa was 35.6%.

Fig. 7 is the filter tube pressure drop at an RFP pressure of 0.60 MPa for a total of 20 cycling times. It shows that the residual pressure drop was stable and did not increase as the filtration time progressed. This shows that, at the RFP pressure of 0.60 MPa, it could

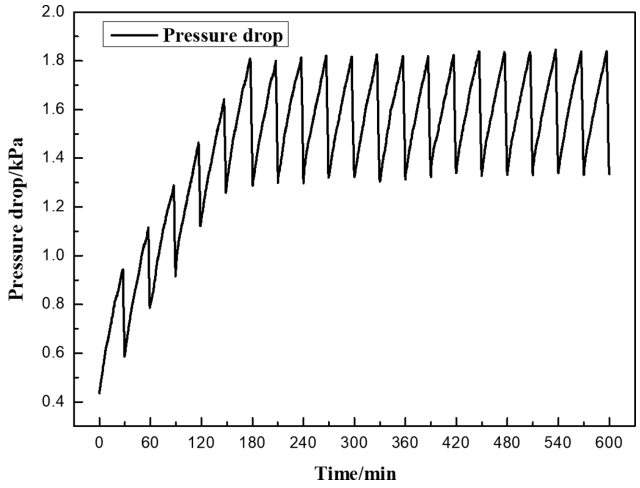

Fig. 6. Influence of 0.45 MPa RFP pressure on pressure drop evolution.

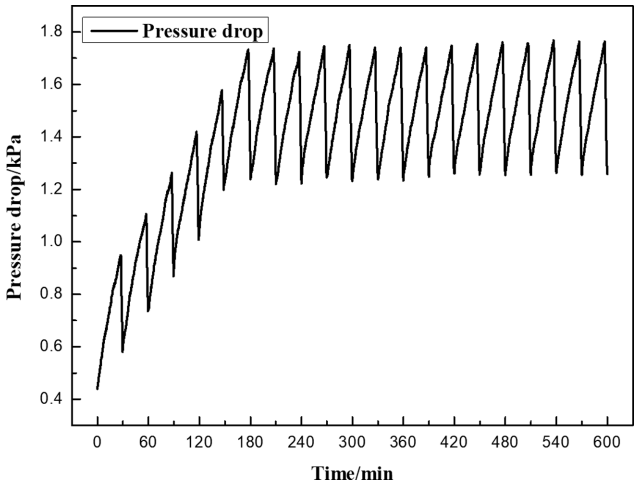

Fig. 7. Influence of 0.60 MPa RFP pressure on pressure drop evolution.

Table 3. Influence of 0.45 MPa RFP pressure on cleaning efficiency

Cycling time	Residual pressure drop (kPa)	Cleaning efficiency (%)	Cycling time	Residual pressure drop (kPa)	Cleaning efficiency (%)
6	1.288	37.3	14	1.341	34.2
7	1.289	36.9	15	1.332	35.6
8	1.298	36.8	16	1.333	35.3
9	1.327	35.1	17	1.332	34.1
10	1.324	35.1	18	1.339	35.4
11	1.316	36.1	19	1.332	35.6
12	1.313	36.0	20	1.335	35.4
13	1.324	35.2			

Table 4. Influence of 0.60 MPa RFP pressure on cleaning efficiency

Cycling time	Residual pressure drop (kPa)	Cleaning efficiency (%)	Cycling time	Residual pressure drop (kPa)	Cleaning efficiency (%)
6	1.239	37.4	14	1.262	36.4
7	1.220	39.1	15	1.260	36.9
8	1.222	38.3	16	1.255	37.5
9	1.252	37.1	17	1.256	37.3
10	1.233	38.7	18	1.263	37.3
11	1.247	37.2	19	1.255	37.6
12	1.234	38.1	20	1.259	37.3
13	1.249	37.1			

meet the cleaning requirement at RFP pressure of 0.60 MPa, and the residual pressure drop was lower than the residual pressure drop when the RFP pressure was 0.45 MPa.

The cleaning efficiency of each cycle at an RFP pressure of 0.60 MPa was calculated using Eq. (2) and shown in Table 4. The residual pressure drop after each cycle at 0.60 MPa RFP pressure was obtained. The average cleaning efficiency at an RFP pressure of 0.60 MPa was 37.5%.

Fig. 8 is the filter tube pressure drop at an RFP pressure of 0.75 MPa for a total of 20 cycling times; it shows that the residual pressure drop was stable and met the cleaning requirement. However, the residual pressure drop was higher than the residual pressure drop when the RFP pressure was 0.60 MPa. Correlation analysis suggested that the entire space of the filter was small, the diameter was only 650 mm, and the pulse jet under the high RFP pressure would cause the dust that had fallen off to be lifted up again. In addition, in the transition process when the pulse jet process came to its end and the filtration process had not been established, the pressure inside the filter tube was lower than the pressure outside the filter tube; the difference related to the RFP pressure, the higher

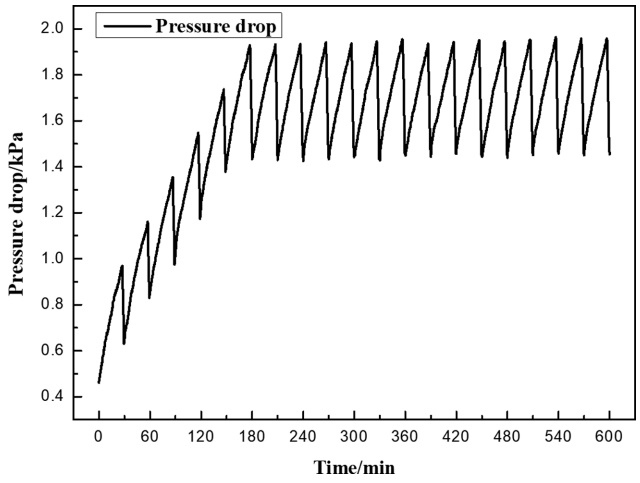

Fig. 8. Influence of 0.75 MPa RFP pressure on pressure drop evolution.

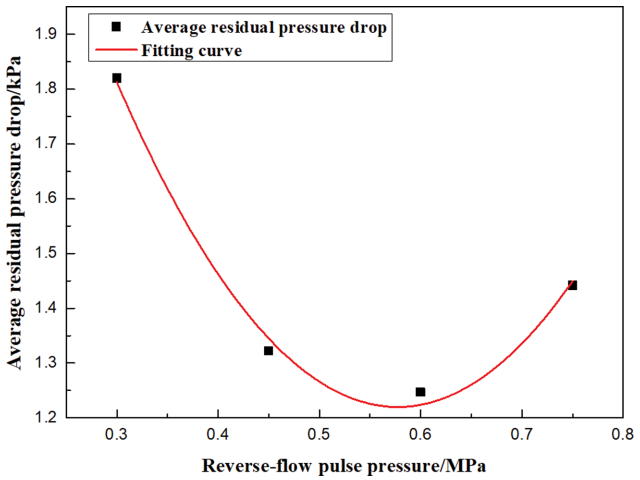

Fig. 9. Average residual pressure drop under different RFP pressures.

Table 5. Influence of 0.75 MPa RFP pressure on cleaning efficiency

Cycling time	Residual pressure drop (kPa)	Cleaning efficiency (%)	Cycling time	Residual pressure drop (kPa)	Cleaning efficiency (%)
6	1.434	32.7	14	1.457	31.8
7	1.429	33.1	15	1.443	33.0
8	1.425	33.4	16	1.439	33.0
9	1.432	33.3	17	1.451	32.6
10	1.442	32.4	18	1.458	32.6
11	1.428	33.7	19	1.450	32.9
12	1.448	32.9	20	1.454	32.4
13	1.444	32.3			

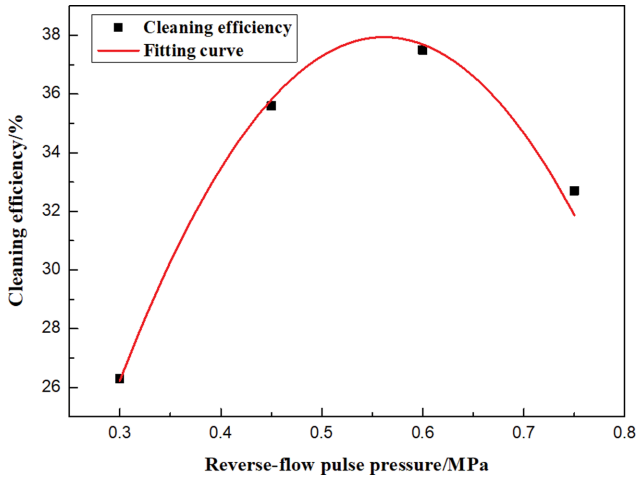

Fig. 10. Cleaning efficiency under different RFP pressures.

the RFP pressure was, the higher negative pressure in the filter tube [16], leading to some of the fine particles being blown off and then redeposited to the filter tube surface, causing cleaning efficiency to be decreased.

The cleaning efficiency of each cycle at the RFP pressure of 0.75 MPa was calculated using Eq. (2) and shown in Table 5. The average cleaning efficiency at an RFP pressure of 0.75 MPa was 32.8%.

After averaging the residual pressure drop values under different RFP pressures, the relationship between the average residual pressure drop and RFP pressure is shown in Fig. 9.

The relationship between the average residual pressure drop and RFP pressure was obtained in Eq. (5) by data fitting.

$$\Delta p_{ra}=7.7p_1^2-8.89p_1+3.79 \tag{5}$$

where Δp_{ra} is the average residual pressure drop.

The relationship between cleaning efficiency and RFP pressures was fitted and shown in Fig. 10. The result is consistent with the results of the Lupion's study [9]; the result indicated that there was a quadratic relationship between RFP pressure and cleaning efficiency, whether at high temperature or normal temperature.

$$\eta=-171.1p_1^2+192.2p_1-16.03 \tag{6}$$

2. Optimization Model

In the actual process, it is desirable to minimize the residual pressure drop and gas consumption, but these goals could not be achieved at the same time. Based on the experimental results, an optimization model was established and shown in Eq. (7).

$$\begin{cases} \Delta p_{ra}=7.7p_1^2-8.89p_1+3.79 \\ G=80.72p_1+6.11 \\ \eta=-171.1p_1^2+192.2p_1-16.03 \\ \min \Delta p_{ra} \\ \min G \\ \text{s.t.}\ \ \eta\geq 25\% \\ \quad 0<p_1\leq 1\ \text{MPa} \end{cases} \tag{7}$$

where the constraint conditions were $0<p_1\leq 1$ MPa and $\eta\geq 25\%$. The objective functions were min Δp_{ra} and min G.

As the meaning and unit of the objective function were different, the residual pressure drop and gas consumption were blurred after using the fuzzy decision method. Objective function satisfaction was taken as the new target value. Satisfaction of the objective function was achieved by calculating and then determining the maximum value for the minimum satisfaction of the objective function [17]. Under the constraint condition, each objective function was assigned an ideal value, an inverse ideal value was obtained to construct objective function satisfaction. The purpose of using the objective function satisfaction was to reflect the satisfaction degree to the target level, thus realizing the fuzzification of the objective function based on the fuzzy compromise algorithm. The variation interval of the fuzzy compromise index λ^* was determined by changing the value of λ^*, such that different optimization results were obtained [18].

The detailed implementation process was:

(1) The satisfaction of the objective function was established to realize unity of the multi-objective function values, the essence being each objective function was close to the optimal value. Therefore, the maximum Z_i^{max} and minimum Z_i^{min} values of each objective function under constraint conditions were obtained and objective function satisfaction was constructed using two extreme ideal values as shown in Eqs. (8) and (9):

$$\begin{cases} z_i^{max}=\max Z_i(x) \\ \text{s.t.}\, g(x)\leq 0 \\ h(x)=0 \end{cases} \tag{8}$$

$$\begin{cases} z_i^{min}=\min Z_i(x) \\ \text{s.t.}\, g(x)\leq 0 \\ h(x)=0 \end{cases} \tag{9}$$

where x is the model variable, $Z_i(x)$ is the objective function, g(x) and h(x) are the constraint conditions.

Then, two extreme ideal values were used to build the objective function satisfaction. Setting the i th objective function satisfaction as μ_i, for the forward objective function, yields Eq. (10)

$$\mu_i=\frac{Z_i(x)-Z_i^{min}}{Z_i^{max}-Z_i^{min}} \tag{10}$$

(2) Multi-objective linear optimization maximum (minimum) operator method. The goal was to maximize the minimum satisfaction in each objective function, letting the two objective functions have a minimum satisfaction of λ. This algorithm guaranteed the fairness of the optimal solution; that is, the maximum satisfaction of all objective functions would not be too large and the minimum satisfaction would not be too small. As shown in Eq. (11):

$$\begin{cases} \max \lambda \\ \text{s.t.}\, \lambda\leq u_i \quad \forall i \\ g(x)\leq 0 \\ h(x)=0 \\ \lambda\in(0,1) \end{cases} \tag{11}$$

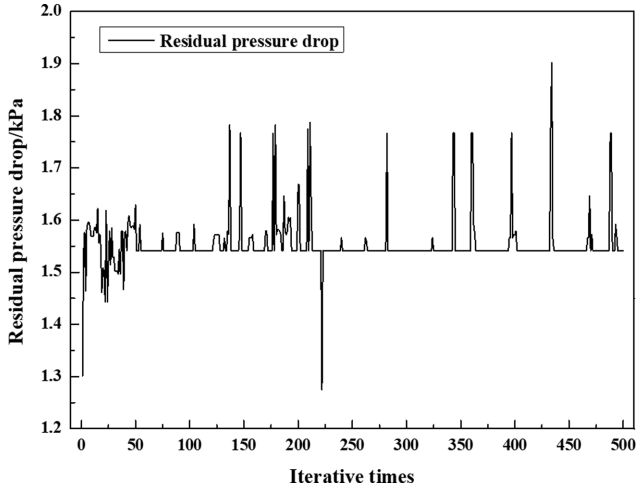

Fig. 11. Calculation results of residual pressure drop.

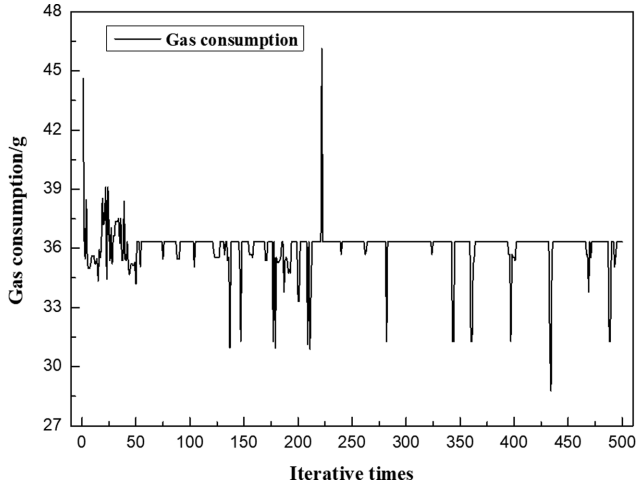

Fig. 12. Calculation results of gas consumption.

where x is the model variable, λ is the objective function. g(x) and h(x) are constraint conditions.

For the model established above, the multi-objective optimization method was used to solve the problem by MATLAB programming. The results obtained are shown in Fig. 11 and Fig. 12.

As can be seen from Fig. 11 and Fig. 12, there was a tendency for the two objective function values: the final optimization result produced a compromise result. At this time, the residual pressure drop Δp_{ra} was 1.541 kPa and gas consumption G was 36.3 g. The corresponding RFP pressure was 0.374 MPa and the cleaning efficiency was 31.9%.

The equation for calculating the standard deviation of the residual pressure drop is as follows.

$$\sigma_1 = \sqrt{\frac{1}{N}\sum_{i=1}^{N}(x_i - \mu_1)^2} \quad (12)$$

where σ_1 is the standard deviation of residual pressure drop, x_i is the residual pressure drop, N is the number of residual pressure drop, 500, μ_1 is the arithmetic mean value.

The standard deviation of residual pressure drop σ_1 is 0.049. Using the same method, the standard deviation of gas consumption σ_2 is 1.214.

CONCLUSION

Long-term experiments were performed using fly ash under normal temperature conditions to investigate the effects of different RFP pressures on the residual pressure drop, cleaning efficiency and gas consumption. When the structural dimensions of the nozzle, pipeline size, and pulse-air tank were constant, gas consumption increased linearly with increased RFP pressure. Within a certain range, cleaning efficiency and residual pressure drop increased and decreased with increased RFP pressure, respectively. When the RFP pressure reached a certain value, cleaning efficiency no longer increased and the residual pressure drop no longer reduced. It was found through linear fitting that there was a quadratic relationship between cleaning efficiency and RFP pressure, with the residual pressure drop as well. A multi-objective optimization model of the ceramic filter was established and solved by fuzzy decision-making method to obtain the optimal RFP pressure by taking the cleaning efficiency as the constraint condition, gas consumption and residual pressure drop as the objective function.

ACKNOWLEDGEMENTS

This research was supported by the National Key Research and Development Program of China (No. 2016YFB0601100).

NOMENCLATURE

G : gas consumption [g]
p_a : absolute pressure of the pulse air tank before pulse jet [MPa]
p_b : absolute pressure of the pulse air tank after pulse jet [MPa]
T_1 : gas temperature before pulse jet [K]
V : volume of the pulse-air tank [m^3]
R : gas characteristic constant [287 $m^2 \cdot s^{-2} \cdot K^{-1}$]
Δp_d : pressure drop of the ceramic filter tubes before pulse jet [kPa]
Δp_a : pressure drop of the ceramic filter tubes after pulse jet [kPa]
Δp_0 : initial pressure drop of the ceramic filter tubes [kPa]
v : filtration velocity [m/min]
Δp_{ra} : average residual pressure drop [kPa]
p_1 : reverse-flow pulse pressure [MPa]

Greek Letters

γ : adiabatic exponent [1.4]
η : cleaning efficiency [%]
λ^* : fuzzy compromise index
λ : minimum satisfaction
σ_1 : standard deviation of the residual pressure drop
σ_2 : standard deviation of the gas consumption
μ_1 : arithmetic mean value of residual pressure drop

RERERENCES

1. S. Heidenreich, *Fuel*, **104**, 83 (2013).

2. F. P. Nagel, S. Ghosh, C. Pitta, T. J. Schildhauer and S, Biollaz, *Biomass Bioenergy*, **35**, 354 (2011).
3. J. D. Chung, T. W. Hwang and S. J. Park, *Korean J. Chem. Eng.*, **20**, 1118 (2003).
4. J. H. Choi, S. J. Ha and Y. O. Park, *Korean J. Chem. Eng.*, **19**, 711 (2002).
5. H. X. Li, Z. L. Ji, X. L. Wu and J. H. Choi, *Powder Technol.*, **173**, 82 (2007).
6. I. Schildermans, J. Baeyens and K. Smolders, *Filter Sep.*, **41**, 26 (2004).
7. J. H. Choi, Y. G. Seo and J. W. Chung, *Powder Technol.*, **114**, 129 (2001).
8. M. Lupión, F. J. G. Ortiz, B. Navarrete and V. J. Cortés, *Fuel*, **89**, 848 (2010).
9. M. Lupion, B. Navarrete, B. A. Fariñas and M. R. Galan, *Fuel*, **108**, 24 (2013).
10. E. Bakke, *J. Air. Pollut. Contr. Assoc.*, **24**, 1150 (1974).
11. J. Ju, M. S. Chiu and C. Tien, *Chem. Eng. Res. Des.*, **78**, 581 (2000).
12. Z. L. Ji, M. X. Shi and F. X. Ding. *Powder Technol.*, **139**, 200 (2004).
13. I. Schildermans, J. Baeyens and K. Smolders. *Filtr. Sep.*, **26**, 41 (2004).
14. C. Kanaoka and M. Amornkitbamrung, *Powder Technol.*, **118**, 113 (2001).
15. H. C. Chi, Z. L. Ji, D. M. Sun and L. S. Cui, *Chin. J. Chem. Eng.*, **17**, 219 (2009).
16. J. P. Hurley, B. Mukherjee and M. D. Mann, *Energy Fuel*, **20**, 1629 (2006).
17. A. K. Dhingra and H. Moskowitz, *Eur. J. Oper. Res.*, **53**, 348 (2012).
18. L. M. Kalonda and R. M. Joseph, *Int. J. Uncertain. Fuzz.*, **21**, 51 (2013).